

# VIDEO-RATE SCANNING PROBE CONTROL CHALLENGES: SETTING THE STAGE FOR A MICROSCOPY REVOLUTION

M. J. Rost, G. J. C. van Baarle, A. J. Katan, W. M. van Spengen, P. Schakel, W. A. van Loo,  
T. H. Oosterkamp, and J. W. M. Frenken

## ABSTRACT

Scanning probe microscopy is at the verge of revolutionizing microscopy once again. Video-rate scanning tunneling microscope (STM) and video-rate atomic force microscope (AFM) technology will enable the direct observation of many dynamic processes that are impossible to observe today, such as atom or molecule diffusion, real time film growth, or catalytic reactions. In this paper we discuss the critical aspects that have to be taken into account when working on increasing the imaging speed of scanning probe microscopes. We highlight the state-of-the-art developments in the control of the piezoelectric scanning elements and describe the latest innovations regarding the design and construction of the whole mechanical loop including new scanner geometries. We identify critical aspects for which no obvious solution exists and aspects where advanced control engineering can help, like piezo non-linearities, the acceleration limit and the challenging technical requirements for the preamplifiers that are needed for measuring a tunneling current. Finally, we provide an overview of a number of new directions that are being pursued to solve the problems currently encountered in scanning probe technology.

**Key Words:** Scanning probe microscopy, video-rate, mechanical issues, control electronics.

## I. INTRODUCTION

Inspired by the pioneering work of Young *et al.* [1], Binnig and Rohrer invented the STM in 1982 [2, 3]. Over the last 25 years, due to its unique capability to observe surfaces in real-space on the atomic scale, scanning probe technology has revolutionized several fields of research, such as surface science and

nanotechnology in general and more particularly film growth, friction, surface chemistry, catalysis, electrochemistry and biology (biophysics). The outstanding versatility of scanning probe microscopes (SPMs) is reflected in many applications that include extreme temperatures [4, 5], truly variable temperature [6], (ultra-high) vacuum or ambient to high pressures [7, 8] and even measurements in electrolytic solutions [9]. Scanning tunneling spectroscopy (STS) at extremely low temperatures [10–14] has greatly enhanced our understanding of local electronic and magnetic properties of surfaces, molecules, and even individual atoms. This has led to new insights in *e.g.* high-temperature superconductivity. In AFM the force between tip and sample, rather than a tunneling current is measured. This allows a wide variety of non-conducting samples to be investigated, with the additional advantage that these can be measured under many conditions,

---

Manuscript received February 16, 2008; accepted August 8, 2008.

All authors are with Leiden University, LION, Niels Bohrweg 2, 2333 CA Leiden, The Netherlands.

M. J. Rost, G. J. C. van Baarle, and T. H. Oosterkamp are also with Leiden Probe Microscopy, Niels Bohrweg 2, 2333 CA Leiden, The Netherlands (e-mail: rost@physics.leidenuniv.nl; baarle@leidenprobemicroscopy.com).

W. M. van Spengen is also with Falco Systems, Gelderlandplein 75L, 1082LV, Amsterdam, The Netherlands.

e.g. in a native liquid environment. Recently, important progress has been made in the sensitivity and speed of AFMs used in liquids [15, 16]. In addition, in industry it is recognized that SPM is a powerful technology: research projects are financed by companies [17] to investigate possibilities for data storage [18], scanning lithography [19], catalysis [20], and quality control [21].

Even though SPM is still a young field, the technology is now on the verge of revolutionizing microscopy again. Increased imaging speed, higher image resolution, and new measurement modes will provide access to new observations in the coming years, thereby providing not only new insights in dynamic processes, but also enabling new applications, such as industrial process control. The figure of merit here is speed (the time to record either a full image or other SPM related information), as it provides access to dynamic processes and uniquely enables studies under realistic conditions. Video-rate SPM technology allows the direct observation of atoms and molecules at work, which will lead to new insights. Speed also increases the user-friendliness of SPM machines: in addition to the immediate gratification of seeing real-time images allowing the user to get direct response to stimuli applied to the system under study, the distortion due to thermal drift is greatly reduced and the images are less sensitive to low frequency vibrations.

In order to further stimulate future activities in this field, we would like to point out the potential impact of *in-situ*, video-rate measurements with some recently reported examples. The growth of thin polycrystalline gold films has been observed during the deposition of several tens of monolayers [22]. These measurements provide unique access to atomic processes that take place during film growth. Using a truly-variable temperature STM [23], it has been possible to follow the structural changes of a polycrystalline network while annealing it to higher temperatures. Even the migration of individual grain boundaries could be resolved [6]. Another striking example is the live observation of a catalyst with near-atomic resolution during a catalytic gas reaction under high pressures and high temperatures mimicking the conditions in which catalysts are actually used [24, 25]. Structural changes of the surface could, for the first time, be correlated with the activity of the catalyst, which led to new insights regarding the well-known gas reaction oscillations [26]. In high-speed AFM the outstanding achievements by Ando and his group [27] are illustrated by their observation of the motion of a kinesin-gelsolin molecular motor over a microtubule [28] and the details of myosin hand-over-hand motion [29].

Over recent years several groups have reported on high-speed SPM activities [30–38]. Significant improvements have been made on the control electronics of SPMs [39–47], the mechanical loop [48], and (piezo-) scanner geometries [33, 34]. Hansma *et al.* recently reported on an AFM system with real video-rate imaging capabilities [49, 50]. Picco *et al.* set a new speed limit with AFM [51], although their measurements were performed without an actively working feedback. This in contrast to Rost *et al.* [40] who obtained line rates up to 10 kHz with a fully functional feedback loop. In this paper we give an overview of the state-of-the-art improvements, we highlight newly identified problems hampering higher scanning speeds, and we indicate directions for possible solutions.

## II. INSTRUMENTATION: ELECTRONICS/SENSORS

### 2.1 SPM control electronics

The feedback of typical SPM control electronics, which accurately regulates the height of the tip, is usually built on the basis of a proportional and integral feedback circuit (PI-regulator). Attempting to speed up SPM measurements requires a control system [41, 52, 53], of which all components (including the feedback electronics) are sufficiently high in bandwidth, provide appropriately high slew rates, and are sufficiently low in noise [54]. In general, these conditions are contradicting, as the noise generated by electronic components increases with the bandwidth  $f_{BW}$  proportional to  $\sqrt{f_{BW}}$  if the noise is white. In reality the noise often increases even faster with bandwidth.

Recently, we reported that it is possible to push the bandwidth of an SPM controller, including the feedback electronics up to real video-rate and even beyond [40]. Instead of obtaining an image within several minutes or tens of seconds, we recorded even up to 200 images per second with fully working feedback. This controller has some unique features, which in combination support real-video measurements and also enhance the overall resolution of the microscope. One of the most important features is the realization of the so-called hybrid mode. This feedback concept, reported for the first time in 1990 [55], allows one to measure intermediately between the two modes that are familiar for STM, namely the constant height mode and the constant current mode. The hybrid mode records not only the height signal of the tip, but also the deviation of the tip with respect to the ideal tip height simultaneously. The operation range of the hybrid mode is typically

limited by the measurement of the tip-sample interaction. In STM, the current must be less than the corresponding maximum voltage of the preamplifier (10 nA in our case) as well as larger than the noise floor again determined by the used preamplifier and the specific setup (see Section 4.1). In contact-mode AFM, the range of the deflection detector is a limiting factor. Depending on the adhesion properties of the sample, a loss of contact may occur with large deviations from the setpoint away from the surface. This can also limit the range of the hybrid mode. In amplitude-modulation AFM, the range over which tip-sample interactions can be measured is approximately equal to the free amplitude of the oscillation.

One should also take into account that, depending on the particular operating conditions, one might influence the sample or the tip even before reaching the physical operation limit of the hybrid mode. Eventually the hybrid mode becomes inaccurate when the operation range is exceeded. Using non-linear gains, one can force the tip height to stay within the operation range even at tip speeds, where one usually would reach the boundaries (see Section 4.3).

We also would like to mention that a quantitative measurement with the hybrid mode is only valid on homogeneous samples.

Fig. 1 shows the working principle: the tip is only following the low-frequency components of the surface structure, largely ignoring the local details. Nevertheless, we obtain full atomic resolution by recording how wrong the tip is positioned with respect to the ideal tip height: we simultaneously measure the so-called  $dZ$  signal that varies linearly in height. Provided a given calibration of the height signal  $Z$ , this  $dZ$  signal can also be accurately calibrated by measuring  $d(dZ)/dZ$  with frozen feedback settings (sample and hold), which is used also for spectroscopic  $dI/dV$  measurements, among other things. In this way, the full information of the surface contour, including all details is given by the addition of the height and error signals  $Z + dZ$ . It is worthwhile to mention here that the RMS value of the error signal of a feedback circuit will, in practice, never reach zero during scanning. This is due to the finite delays within the total loop, like the mechanical inertia of the piezo element. This also implies that standard electronics always miss information on the real surface topography resulting in a measurement error. The hybrid mode also adds user comfort, as the sharpness and, therefore, the details of the images depend much less on the feedback settings (proportional and integral gain as well as filters) of the user. If the gains of the feedback are set *too low* (in order to follow all surface details) but still high

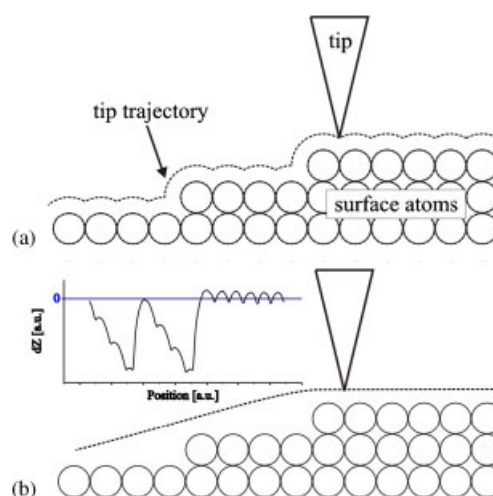


Fig. 1. STM feedback modes: (a) usual 'constant current mode'; the tip follows every detail of the surface corrugation, and (b) the 'hybrid mode' [40], in which the tip follows only the 'macroscopic' surface structure, while the deviation of the tip height from the ideal height is simultaneously recorded via the so-called  $dZ$  channel. Every surface detail is captured independently of how faithfully the tip follows the surface structure.

enough to avoid surface or tip changes, the information is not lost but simply transferred into the  $dZ$  signal. As long as the combination of tip speed and feedback settings are such that a destructive tip-surface contact and complete contact loss is avoided, one always retrieves the complete surface information, limited only by the sharpness of the tip and the cleanliness of the sample.

In addition to this hybrid-mode feedback, we have implemented a variable low-pass filter within the feedback loop that influences only the cut-off frequency. The low-frequency gain of this filter is one, independent of the filter setting. Using this filter with optimal feedback settings (optimal P- and I-gains), one can adjust the frequency response of the tip reaction, thereby smoothly tuning the overall feedback behavior to all intermediate states between pure constant current and constant height modes.

It is important to realize that the total tip movement as well as the accelerations are significantly reduced in the hybrid mode in comparison to the constant current mode: higher frequencies are avoided. In terms of frequency response, the constant height mode would, theoretically speaking, be ideal. However, it is applicable only to flat terraces of single-crystal surfaces with no or only modest height variations. Using the constant height mode, one can usually cross one or two single atomic height steps without risking tip-sample contact. The hybrid-mode provides the opportunity to maximize the scanning speed also on rough surfaces, like on

Table I. Key specifications of the control electronics as described in [40]. This set of electronics is commercially available at Leiden Probe Microscopy (LPM) [56].

Scan generator: (capable of measuring in an analog mode as well as in a digital mode)	<p><i>Analog:</i></p> <p>Line rates up to 10.2 kHz. Adjustable parabolic rounding of the scan signal. Option for real sine-wave scan generation. Hardware background and tilt subtraction. Online zooming, panning, and rotating.</p> <p><i>Digital:</i></p>
Max. data transfer speed	<p>Shortest time for setting and reading a pixel: 30 <math>\mu</math>s. 13 Msamples/sec. in total. The maximum transfer speed for each ADC is 4 Msamples/sec. We can simultaneously record 4 ADCs with 2.1 Msamples/sec.</p>
ADC resolution (up to 8 ADCs simultaneously)	<p>16 Bits. At low data speeds, each sample is usually 8 times oversampled within the ADCs in order to reduce effects of bit flipping. This ensures a full 16 bit resolution. (Additional oversampling as standard in common controllers is also possible via the software.) Additional input gains: 1x, 2x, 4x, 8x, 16x, 32x, and 64x.</p>
Feedback bandwidth:	<p>As, in our case, the closed-loop feedback bandwidth is usually limited by the mechanical behavior of the (piezo) scanner, the following list provides an overview on the measured open-loop bandwidth of the individual components of the feedback. The bandwidth is measured at the <math>-3</math> dB point, if not stated differently.</p>
STM-input stage	<p>Consists of an absolute value amplifier and logarithmic amplifier that covers 4 decades (<i>e.g.</i> a corresponding range from 0.001 to 10 nA), for the linearization of the tunnel current: 1 MHz.</p>
AFM-input stage	<p>Photodiode for cantilever deflection: 12 MHz. with 10 fm/<math>\sqrt{\text{Hz}}</math> noise from 1 kHz &lt; <math>f</math> &lt; 5 MHz Amplitude and phase detector for dynamic modes: 7 MHz with a propagation delay of half a period</p>
I-Gain	between 240 Hz and 47 kHz at 0 dB
P-Gain	between $-80$ dB and 0 dB up to 1 MHz
Low-pass filter	1–100 KHz (see text)
50 kHz PreAmplifier	<p>The preamplifiers and high voltage drivers are listed separately in the table. Gain: <math>10^9</math> V/A. Integrated input current noise &lt; 0.03 nA with <math>C_{\text{input}} = 27</math> pF</p>
600 kHz PreAmplifier	<p>Gain: <math>10^9</math> V/A. Integrated input current noise &lt; 0.1 nA with <math>C_{\text{input}} = 27</math> pF</p>
High-Voltage Drivers	<p>Adjustable gain between 15x and 19x. Output voltage <math>\pm 190</math> V. Small-signal bandwidth: 400 kHz with <math>C_{\text{load}} = 1.5</math> nF. Full-power bandwidth: 60 kHz with <math>C_{\text{load}} = 1.5</math> nF. Slewrate: 75 V/<math>\mu</math>s up to loads of <math>C_{\text{loadt}} = 1.5</math> nF. Slewrate: 50 V/<math>\mu</math>s up to loads of <math>C_{\text{loadt}} = 4.7</math> nF. Hum (50 Hz): 3 <math>\mu</math>V rms. Integrated noise with 400 kHz bandwidth: 0.3 mV rms.</p>

polycrystalline or biological samples. The importance and the impact of the reduction in total tip movement on speed and resolution of the microscope will become obvious in Sections III and IV where we discuss non-linear coupling effects of scanning piezo elements.

The realization of this control system [40] has required extreme designs: we have pushed several aspects to the limits of what was technically feasible

including analog, digital as well as programmable electronics, data transfer, and data storage. If one desires to reach real video-rate imaging with 25 images/sec., each containing  $512 \times 512$  pixels, the requirements on the electronics are: 6.5 Msamples/sec., a line rate of 12.8 kHz, and a closed-loop bandwidth of the feedback of more than 1 MHz (assuming 100 atoms per line). The above table highlights our key specifications

demonstrating also the necessity for further improvements (Table I).

When imaging soft biological samples with AFM, the height difference is usually much larger than in typical STM experiments. A microtubule, for example, is a hollow cylinder with a diameter of approximately 20 nm that may easily collapse if the applied imaging force exceeds 400 pN. In order to keep the tip-sample interactions to a minimum, one should, first, choose the setpoint height closer to the loss-of-contact point and, second, avoid excursions of the tip from the desired height in the direction towards the surface. Larger gains will diminish both the amplitude and the duration of excursions from the set height, thereby lowering the risk of both the loss of contact and too strong an interaction. However, the gains cannot be increased indefinitely, as the feedback circuit will become instable at some point and will start to oscillate (typically at a piezo resonance frequency).

In order to reduce this effect, Ando *et al.* have implemented a clever active damping scheme [57]. Another important realization, which improves the feedback response, is that temporarily larger gains may be used whenever the error signals are large, as long as the gains are reduced again when the error signal is small. This requires the implementation of a dynamic proportional-integral-differential (PID-) controller [58]. In Section 4.3, we demonstrate the necessity for such a solution. In order to further minimize the error signal the group of Ando has implemented a feedforward scheme [59], in which the information contained in a previous scan line is used for pre-control in anticipation of the following scan line.

## 2.2 High-speed aspects in scanning tunneling spectroscopy

In general, the bandwidth of the STM current is limited by the physical tunneling rate of electrons from tip to sample. For normal tunneling currents, *e.g.* 1 pA, the tunneling rate is still more than 6 MHz, far above the bandwidth of amplifiers that could measure such a small current.

Scanning tunneling spectroscopy (STS) is a very powerful tool to obtain fundamental insights in electronic as well as magnetic properties of surfaces [10–14]. The drawback of this technique is the extremely long acquisition time needed to obtain an image with a reasonable number of data-points. Similar to the force-volume mode in AFM, a complete STS map requires many current readings at different voltages for each individual pixel of the map. If one would like to measure a map of only 100 by 100 pixels and

50 different voltages per pixels within one second, this would require a data transfer rate of 500 ksamples/sec. Although this number is easily achievable with the electronics described above, which can reach data transfers up to 13 Msamples/sec, there is still a problem related to the preamplifier. STS measurements often require an fA range sensitivity, which implies a dramatically reduced bandwidth of the preamplifier, usually down to only few kHz or less. Assuming a bandwidth of only 1 kHz, the above measurements would last 8 minutes. Scaling to full resolution (512 × 512 pixels and 100 volt steps), a measurement would last 7 hours. Improvements on the preamplifiers would, therefore, not only enable faster imaging, but would also significantly reduce spectroscopic measurement times.

## 2.3 High-speed aspects in AFM: cantilevers

In AFM, the tip-sample force is measured by a cantilever force-sensor: a small mechanical structure with a useful bandwidth that is limited by its resonant behaviour. The resonance frequency of a clamped-free, rectangular cantilever of width  $W$ , length  $L$ , thickness  $T$ , made of a material with density  $\rho$  and Young's modulus  $E$ , is given by  $f_0 = (1.02/2\pi)(E/\rho)^{-1/2}(T/L^2)$ , while its spring constant is given by  $k = 0.25 * EW(T/L)^3$  [60].

The maximum achievable imaging speed of an AFM can be limited by the bandwidth of the cantilever. The exact relation between cantilever resonance frequency and the cantilever-imposed limit of the tip-sample measurement bandwidth depends strongly on the mode of operation and the detection method, but it is always proportional to the resonance frequency  $f_0$ .

For amplitude modulation AFM, the bandwidth is usually taken as  $f_0/Q$  (resonance frequency/quality factor), although a recent study by Kokavec *et al.* [61] reveals that this bandwidth also depends on the amplitude setpoint. When using contact mode with a large force setpoint, the cantilever is operated in a clamped-pinned configuration and the resonance frequencies are approximately one order of magnitude higher. However, this type of operation increases the risk of tip wear and sample damage.

Currently, resonance frequencies of commercially available AFM cantilevers vary from a few kHz to around 1 MHz. The variation in resonance frequencies is mainly realized by a variation in the spring constant. However, to keep the interaction forces low during fast scanning, *i.e.* to increase the resonance frequency without increasing the spring constant, the cantilever size should be reduced in all its dimensions. Pioneering work in the miniaturization of cantilevers

has been done by the Hansma group [62–65]. They fabricated silicon nitride cantilevers with integrated tips: very soft ones (5 mN/m; 25  $\mu\text{m}$  long) with a resonance frequency of 350 kHz as well as reasonably soft ones ( $< 2 \text{ N/m}$ ; 10  $\mu\text{m}$  long) with resonance frequencies up to 2 MHz. All cantilevers were 10  $\mu\text{m}$  wide and 100 nm thick and their resonance frequencies were determined in air. Kitazawa and co-workers from Olympus, collaborating with the group of Ando, fabricated silicon nitride cantilevers with integrated tips [66]. These cantilevers had dimensions of 10  $\mu\text{m} \times 2 \mu\text{m} \times 0.1 \mu\text{m}$ , spring constants of around 0.2 N/m, and resonance frequencies of 1.2 MHz measured in water. The resonance frequency in water is typically three times lower than in air, due to the mass of the liquid, that has to be moved with the cantilever. The exact differences can be calculated by the use of hydrodynamic theories [67]. As the reduction of resonance frequencies is lower for narrower cantilevers Katan and Oosterkamp [68] produced silicon cantilevers with a width of only 1.7  $\mu\text{m}$  by means of focused ion beam (FIB) milling. These cantilevers had a spring constant of 2 N/m, and resonance frequencies of 1.8 and 1.2 MHz in air and liquid, respectively. For vacuum operation, one can benefit from cantilevers with low internal dissipation; therefore, single crystal silicon is the material of choice. Yang and co-workers [69] fabricated miniature cantilevers (11.5  $\mu\text{m} \times 4.16 \mu\text{m} \times 0.2 \mu\text{m}$ ) from this material. They achieved a quality factor of 19000 in vacuum with a spring constant of 1 N/m.

### III. INSTRUMENTATION: MECHANICAL HARDWARE/PIEZO ELEMENTS

At first sight, one is tempted to think that most speed problems are solved with the realization of the SPM control electronics described above. Indeed, in comparison to standard controllers, we are able to increase both the speed and the resolution of existing microscopes significantly, but the maximum achievable speed is still not sufficient for monitoring fast dynamic processes on surfaces. It is limited by the non-ideal behaviour of piezoelectric elements used for scanning the tip over the sample. In Section III, we describe the underlying reasons and point out the importance of the precise knowledge on the behaviour of the piezo scanning elements.

#### 3.1 Closed-loop tunneling spectrum of a usual tube scanner

To pinpoint the fundamental problem of state-of-the-art SPM technology, we have used our electronics

to measure the Fourier transform of the tunneling current while hovering above a particular point on the surface without scanning. This ensures a clean spectrum without any frequencies originating from the scanning motion or the feedback related height variation of the tip when following the surface structure. Driven by the noise of the drivers, this method measures the spectrum of the closed-loop system, which is at most linear up to  $\sim 90\%$  of the Z-resonance frequency of the piezo element. In addition, lower frequency modes of the piezo element, like the bending mode, couple in the closed-loop and deteriorate the linear regime around these frequencies. For a quantitative analysis, one should take into account that these spectra are measured behind the 50 kHz preamplifier and, therefore, before the log-amplifier of the STM-input stage, which naturally implies non-linear components of a perfect sine variation of the tip-sample distance. The scanner used in this subsection is built from a EBL#2 piezo tube [70] with the following dimensions: height 12.7 mm, outer diameter 7.6 mm, and inner diameter 6.3 mm. Fig. 2(a) shows the Fourier transform of the tunneling current when using stable, non-resonant, tunneling conditions.

Several peaks can be identified that are all related to the resonance frequencies of the scanning tube that carries an additional load of approximately 0.1 g in the form of the tip and the tip holder. The tip holder consists of two metal shielding plates made from tantalum and an injection needle capillary, which are all held together via some ceramic parts. In order to reduce the weight,

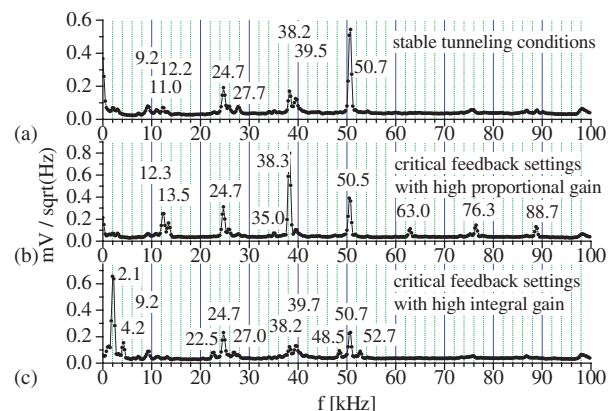


Fig. 2. Fourier transform of the tunneling current (a) with optimal tuned, stable feedback settings (P gain, I gain, and filters), (b) with critical feedback settings for high frequencies (high P gain), and (c) with critical feedback settings for low frequencies (high I gain). These measurements are very sensitive to the resonance frequencies of the mechanical loop. Please notice also the indications for a non-linear coupling of the piezo movements (see main text).

these ceramics are fabricated from boron-nitride. The frequencies obtained fit nicely with those measured using a lock-in technique, as is described in [40]. It is also noticeable that the measurements presented here show a much higher resolution as well as better sensitivity for measuring the piezo resonance frequencies when compared to the work reported in [40]. Due to this increased sensitivity, we are now able to detect more peaks, enabling us to more clearly identify the individual modes of the piezo. In [40], we erroneously identified the 39 kHz peak with the longitudinal mode ( $Z$ -height direction) of the piezo tube, but the improved spectra of Fig. 2 reveal that a slightly different interpretation is required. In agreement with our earlier paper, we find two peaks around 9 kHz that correspond to the first bending modes ( $X$  and  $Y$ ) of the tube which has a broken rotational symmetry due to asymmetry in the tip holder. We find the first torsional mode, again in good agreement, at 24.7 kHz. The peaks at 38.2 kHz and 39.5 kHz, however, correspond to the second bending mode of the tube again split due to the broken symmetry. The real longitudinal mode of the tube ( $Z$ -height-direction) lies at 50.7 kHz, which is confirmed by the large peak height. As we are actively regulating the tip height in  $Z$  with the feedback system, we are most sensitive to this mode.

Starting with stable tunneling conditions, as illustrated by Fig. 2(a), one can identify problems with respect to the mechanical loop at higher frequencies, by increasing the overall gain of the feedback for higher frequencies. With a fixed integral gain, this can be achieved by increasing the proportional gain ( $P$ -gain). Similarly, one can identify low frequency problems with an increase of the integral gain ( $I$ -gain). Fig. 2(b) shows the Fourier transform of the tunneling current with an increased  $P$ -gain, tuned such that the feedback loop was at its critical point, *i.e.* just before becoming unstable. There are two obvious changes with respect to the spectrum in Fig. 2(a): the highest peak has changed from 50.7 kHz to 38.2 kHz and several peaks appear that are equally spaced. With higher  $P$ -gain, the feedback adjusts the variations in the  $Z$ -mode (50.7 kHz) more precisely, which leads to a slight decrease of the peak height from 0.54 mV/ $\sqrt{\text{Hz}}$  down to 0.39 mV/ $\sqrt{\text{Hz}}$ . Simultaneously, one notices a dramatic increase in amplitude of the second bending mode in the  $X$ -direction at 38.2 kHz. There are two explanations for this observation. One is that the overall feedback settings might exceed the stability criterion of the closed feedback loop for this particular frequency. The other possibility is based on the tilt of the sample, roughness, or variation in electronic corrugation along the  $X$ -direction. Taking into account the noise vibrations of the scanner,

a sample tilt can induce a tunneling current variation. The feedback is able to compensate for this by moving the tip (in height) with exactly the same frequency as the (noise) vibration. Assuming a non-linear coupling of the piezo motion in different directions\*, this would lead to an enhancement of a particular vibrational mode, in this case the vibration in the  $X$ -direction. More evidence for the existence of non-linear coupling is given by the other peaks. A careful inspection of their frequencies shows that the frequency difference between the second  $X$ -bending mode and the  $Z$ -height-mode leads to satellites above and below several of the harmonic (*i.e.* linear) eigenfrequencies of the system: (50.5 – 38.3 = 12.2) kHz; the bare 12.3 kHz is visible as well as (50.5 + 12.3  $\approx$  63.0) kHz, (63.0 + 12.3  $\approx$  76.3) kHz, and (76.3 + 12.3  $\approx$  88.7) kHz. Moreover, the frequency difference between the second  $X$ -bending mode (38.3 kHz) and the torsional mode (24.7 kHz) is also visible as a new frequency vibration at 13.5 kHz. As confirmed in the following section, these observations strongly suggest a non-linear coupling of all movements of the piezo element.

When increasing the gain at low frequencies by increasing the  $I$ -gain, we obtain the spectrum shown in Fig. 2(c). The highest peak, at 2.1 kHz, is a drum-mode related to our sample holder (effectively the sample is moving up and down). This spectrum reveals even stronger indications for non-linear coupling: both  $Z$ -height related modes, the torsional mode at 24.7 kHz as well as the  $Z$ -height mode at 50.7 kHz now show satellite peaks at higher and lower frequencies that are exactly 2.1 kHz apart from their original modes.

One might argue that the observed non-linearity stems solely from the fact that the measurement was performed on the signal before it was linearized by the log-amplifier. However, based on a calculation, in which we fit the non-linearity of the tunneling junction with the measurements, we can conclude that the measured non-linear peak heights exceed the calculated values by a factor of 3. At most, 30% of the peak heights are due to the measurement performed before the log-amplifier. The remaining 70% are probably due to the non-linear coupling of the piezo element, for which we provide additional proof in the next subsection.

This non-linear coupling of the piezo motion may cause artifacts during scanning. Imagine what happens during scanning along the  $X$ -direction with atomic

\*Strictly speaking, an alternative explanation is possible, namely that an applied offset voltage makes the scanner not be at its center (0,0). As the tube is bent, a height correction can excite a bending resonance.

resolution in constant current mode. The tip is moved up and down with the ‘atomic frequency’ ( $X$ -scan speed divided by the lattice constant), which is usually much lower than the frequency of the  $Z$ -height resonance of the scanner. However, when this frequency of passing atoms coincides with the first bending resonance frequency of the piezo element and there is (non-linear) coupling between the  $Z$ - and  $X$ -modes of the piezo element, the bending resonance along  $X$  can be excited, which can even lead to a resonance catastrophe. In the following section, we provide direct proof for the presence of this non-linear coupling by quantifying the non-linear coupling terms.

### 3.2 Quantification of the non-linearity for a conical piezo

In the previous section, we demonstrated that the tunneling current can exhibit non-linear effects. One of the suggested sources for this non-linearity is the piezo-electric scanning element. These types of actuators are known to show non-linear behavior such as hysteresis and creep. In order to prove that it is indeed the piezo element that causes the satellite peaks in the Fourier transform curve of Fig. 2(c), and not, for example, the electronics or other mechanical structures in the system, we performed the following experiment. We mounted a conical piezo-actuator, which is described in more detail in Section 3.3, on a simple, rigid support (not an SPM). The electrodes of this conical piezo, which had been machined from a solid piece of EBL#2 material [70], were segmented into four symmetrical electrodes on the outer wall ( $X+$ ,  $X-$ ,  $Y+$ ,  $Y-$ ) and 1 single electrode on the inner wall ( $Z$ ) (see Fig. 3a). While the  $Y+$ ,  $Y-$  and  $Z$  electrodes were grounded, the sum of two sine waves was applied to the  $X+$  electrode:  $S_1(A_1, f_1) + S_2(A_2, f_2)$  with the  $A$ ’s denoting the two amplitudes and the  $f$ ’s the frequencies. We set the amplitude  $A_1$  to 35 V and the frequency  $f_1$  such that it matched the bending resonance frequency of the piezo: 48.5 kHz. We varied the amplitude of the second signal,  $A_2$ , between 0 V and 80 V while we kept the frequency,  $f_2$ , fixed at 55 kHz. Information on the mechanical response of the piezo actuator can be obtained by performing a fast Fourier transform (FFT) on the current flowing from the  $X$ -electrode to ground (see Fig. 3). It is important to realize that, in principle, one should account for the fact that the signal of interest is measured via the transfer of a high-pass filter below its filtering frequency, as illustrated in Fig. 3(b). The linearity of the filter, however, affects only the individual peak amplitudes that will be measured by the FFT analysis. As one can correct for this effect by multiplying the

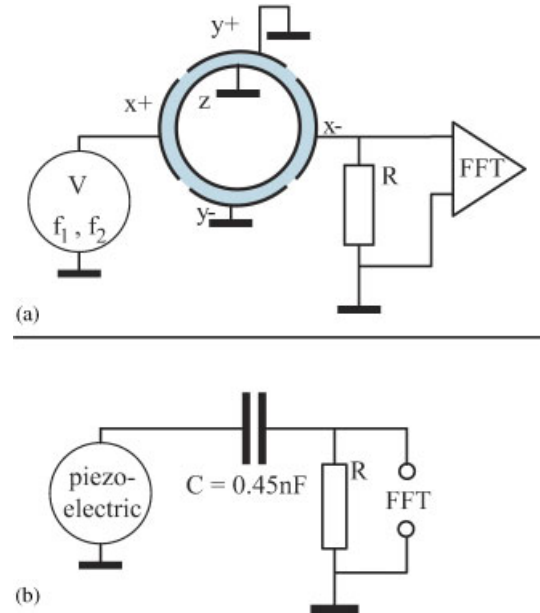


Fig. 3. Connection schemes: (a) for the measurement of the non-linear response of the piezo-actuator, and (b) the equivalent electrical circuit for the readout part showing that the signal experienced high-pass filtering due to the RC-filter. As the resistance used was 512  $\Omega$  and the capacitance of the piezo was measured to be 0.45 nF, the cut-off frequency ( $1/RC$ ) was 4.3 MHz.

measured signals with the inverse transfer function of the high-pass filter (constant factor at each frequency), we can safely ignore this effect here. In addition, we ensured that the signal generators and high-voltage amplifiers used in this measurement were all sufficiently linear so that the non-linearities introduced by these devices were negligible.

In Fig. 4, we show measurements at different amplitudes  $A_2$ , while all other parameters in the experiment were kept constant. Starting with  $A_2$  equal to zero (top panel), we gradually increased  $A_2$  from the top panel down to the lowest panel. Please note that we also detect the first harmonic,  $2f_1$  next to the bare frequency of  $f_1$  in the top panel. On increasing  $A_2$ , we observe the generation of many related frequencies.

These observations can directly be attributed to non-linear effects: driving a non-linear piezo-electric actuator at two different frequencies will not only result in a mechanical response at those two specific frequencies, but will also show a response at super- and subharmonic frequencies such as  $f_2 - f_1$ ,  $f_1 + f_2$ ,  $2f_1 + f_2$ , etc. One can easily find expressions for the expected amplitude dependence of the generated super- and subharmonic signals on the applied amplitudes  $A_1$  and  $A_2$ ;

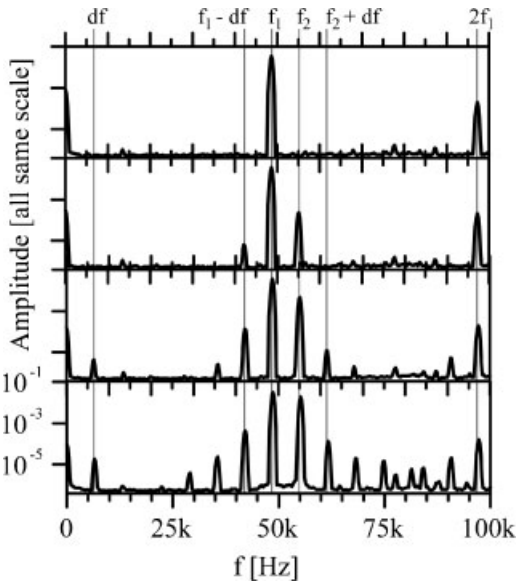


Fig. 4. Selection of measured FFT-graphs. The amplitude  $A_2$  of the signal  $S_2$  was varied, while all other parameters, *i.e.*  $A_1$ ,  $f_1$  and  $f_2$ , were kept constant. The non-linear transfer of the original signals is clearly visible at the frequencies  $2f_1$ , the difference frequency  $df = f_2 - f_1$ ,  $f_1 - ndf$  and  $f_2 + ndf$ , with  $n$  being an integer number.

examples are:

$$A(df) = C_1 A_1 A_2 \cos(2\pi df t) \quad (1)$$

$$A(f_1 - df) = C_2 (A_1)^2 A_2 \cos[2\pi(f_1 - df)t] \quad (2)$$

$$A(f_2 + df) = C_3 A_1 (A_2)^2 \cos[2\pi(f_2 + df)t] \quad (3)$$

where the difference frequency is  $df = f_2 - f_1$ .

From the measured data presented in Fig. 4, we have obtained these dependencies, as shown in Fig. 5. The red lines represent fits based on the above expressions: linear or quadratic. The observation that these curves are indeed close to the expected linear and quadratic behavior, serves as direct evidence that in addition to the intended motion at the driving frequency the piezo scanning element shows significant motion at frequencies that are related the driving signals, but also clearly differ from them. The additional response can be found at exactly the frequencies that are generated by the piezo non-linear effect.

### 3.3 Alternative geometries

The tripod scanners of the early days of scanning probe microscopy have been replaced by tube scanners, as these have higher resonance frequencies. A review paper on tube scanners has been published recently by

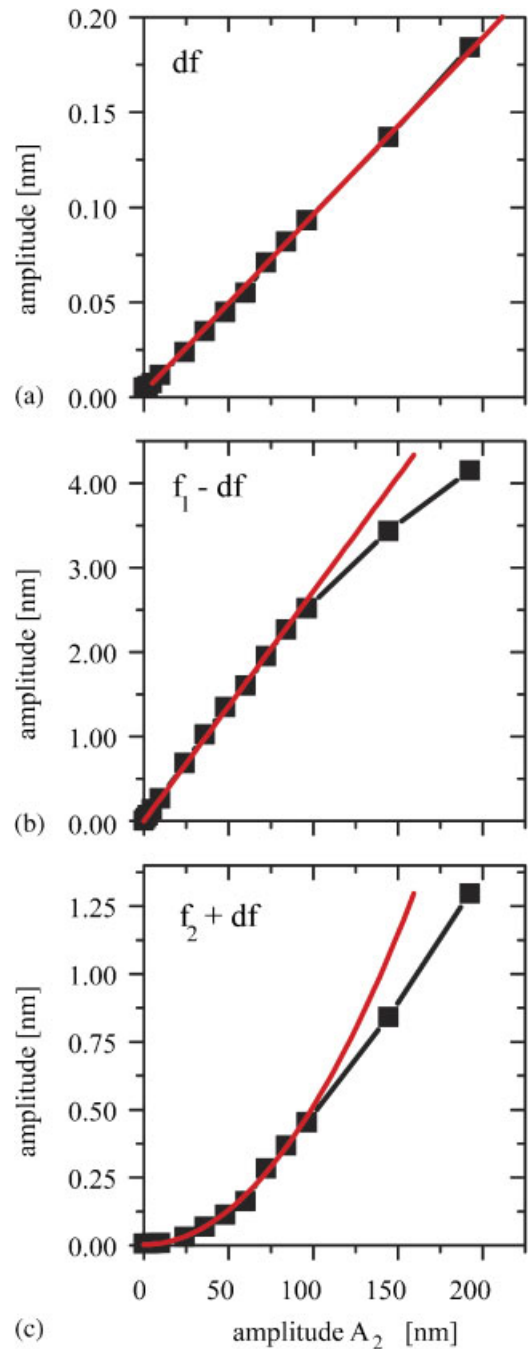


Fig. 5. Amplitudes for various frequencies as a function of the applied amplitude  $A_2$ . The red (grayish) lines represent fits: linear and quadratic as expected from the theoretical expressions, see equations above.

Moheimani [71]. Straightforward sectioning of the outer electrodes into four quadrants turns the whole tube into a rigid-body XYZ scanner. However, a tube is not the most optimal geometry, if speed is the main concern. When modest scan ranges are sufficient for an SPM

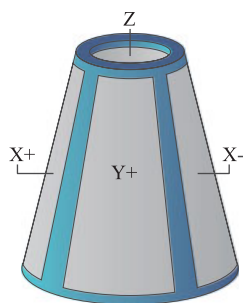


Fig. 6. Geometry of a cone-shaped piezo-actuator.

application, actuators can be built from stacks of thickness- and shear-mode piezo plates thereby achieving even higher resonance frequencies than piezo tubes [40].

A conical piezo geometry as shown in Fig. 6, presents another way of producing a stiffer scanner with a high resonance frequency, while simultaneously keeping a sufficiently large scan range. The main idea behind this design is twofold. The first advantage of a cone is that the triangular aspect of this shape makes the structure stiffer than a traditional tube, since the triangular cross sections of this device are very rigid and difficult to bend or shear, in contrast to rectangular cross sections of a tube. The second advantage is that the parts that are moving with the largest amplitude are located near the apex of the cone and thus have a relatively low mass. The combination of the increased stiffness and the decreased (effective) mass indeed leads to significantly increased resonance frequencies of these cones.

Using finite element analysis, we have investigated various cone scanners with different shapes and dimensions. In the following, we present some preliminary results on a particular choice of dimensions for the cone. More detailed information on the calculation and results, such as the delicate balance between the scan range and resonance frequency, will be published elsewhere [72]. The conical piezo, which was used in the experiments described, was produced by Leiden Probe Microscopy [56], which offers cones with any desired angle and dimension. We used a cone with a height of 7.4 mm, a cone angle of  $35^\circ$  and a wall thickness of 1 mm. For this geometry, we calculated a lowest resonance frequency of approximately 45 kHz (bending mode) and scan ranges close to  $1 \mu\text{m}$  in the  $X$ - and  $Y$ -directions and 500 nm in the  $Z$ -direction.

Fig. 7 shows the result of a lock-in measurement performed analogous to the method described in [40]. This measurement confirms our calculations: the first natural resonance frequency lies at approximately 47 kHz. By performing a real STM experiment on a single crystal Au(110)-surface in ultra-high vacuum we

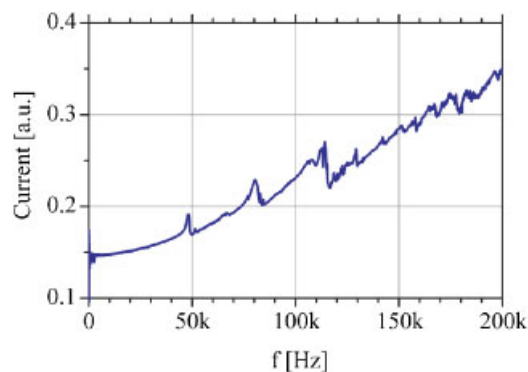


Fig. 7. Natural resonance frequencies of the conical actuator as described in the text. This curve is measured by means of the lock-in technique described in [40]. The peaks verify the predictions obtained from the finite element analysis calculations: the first bending resonance is at  $\sim 47$  kHz, and the first  $Z$  resonance at  $\sim 70$  kHz.

measured the  $X$ - $Y$ - $Z$  ranges and found that these match the calculated values. In addition, by performing scans with almost the maximum scan range, we have verified that the unconventional shape of the actuator does not introduce new image distortions. In conclusion, conical piezo geometries are ideally suited for high-speed measurements with scan-ranges up to  $\sim 1 \mu\text{m}$ . In addition, the open geometry of the conical piezo maintains the advantages of the typical cylindrical tubes above the stacks: signal cables and optical fibres can be mounted easily through the center of the actuator.

In order to achieve larger scan ranges (approximately 10 micrometers) in combination with high resonance frequencies several research groups have demonstrated the feasibility of implementing piezo stacks into special geometries that decouple the  $X$ ,  $Y$ , and  $Z$  motions of the actuator (often referred to as flexure stage scanners) [16, 33, 34, 51, 73–75]. Fukuma *et al.* have realized a stack scanner with a  $Z$  resonance frequency of 540 kHz [76]. Another advantage of flexure stage scanners is that relatively heavy masses can be actuated, like samples, while still achieving high resonance frequencies (tens of kHz).

The Miles group in Bristol pioneered the use of resonant scanning for SPM purposes [36]. They used a quartz tuning-fork oscillator to generate the fast scanning motion. Instead of avoiding the resonance frequency of the scanner, they use exactly this frequency to excite it. This allows scanning of light samples with large scan ranges in combination with line rates up to 30 kHz [77]. Resonant scanners offer high scan speeds, but at the cost of severely limited flexibility. The high quality factors of these scanners prevents from useful scanning at slower line rates than the resonance. Furthermore, height feedback is impossible in the

particular chosen geometry. Nevertheless, it has been shown that soft samples can be imaged non-destructively without feedback, if scan speeds are sufficiently high [78].

In our opinion, a conical piezo element (or a MEMS scanner, see below) is the best choice for scanning a light object, like the tip. If one desires to scan the sample, the flexure stage scanner might be the more appropriate choice.

## IV. OPEN PROBLEMS

### 4.1 Preamplifier noise for STM and STS

As the effort spent on control electronics results in a continuing decrease in noise in the feedback path and the actuators continue to increase in resonance frequency, the measurement of the tunnel current becomes a severe limiting factor for an STM. Ideally, the ultimate electronic bandwidth in STM should be limited by the shot noise in the tunneling current only. One can easily calculate the shot noise,  $I_n$ , integrated over a bandwidth from DC to a maximum bandwidth,  $f_{BW}$ , as,  $I_n = \sqrt{2eI_t f_{BW}}$  and compare this value to a typical tunnel current  $I_t$ . For a tunnel current of 1 pA or 1 nA, the bandwidth at which  $I_n$  becomes equal to  $I_t$  is 3 MHz or 3 GHz, respectively. However, in order to achieve this, one would need a current measurement over which the entire bandwidth has a noise floor below 0.5 fA/ $\sqrt{\text{Hz}}$  or 20 fA/ $\sqrt{\text{Hz}}$ , respectively. At present current to voltage converters usually have a room temperature feedback resistor of at most 1 G $\Omega$ , leading to a low frequency noise of 5 fA/ $\sqrt{\text{Hz}}$ . However, above a certain corner frequency, the noise grows linearly with the frequency. This corner frequency typically is a few kHz and depends on the cable length between the tunneling tip and the converter (input capacitance) and on the noise of the transistor of the operational amplifier, which is used in the main stage of the current to voltage converter. Often, the input capacitance is, therefore, the limiting factor. This effect is called noise gain in the electronic engineering community.

Although the noise of transistors has been slowly decreasing in recent decades, large bandwidth current to voltage converters that are based on transistors will be far away from achieving the ultimate shot noise limit for a long time to come. Applying SQUID electronics to the measurement of tunnel currents may provide an alternative, but there are still major hurdles to be taken to make this practical [79]. Such a preamplifier would definitively be interesting for the application of STS measurements at low temperatures, where long cables down to the cryostat imply high input capacitances.

Moreover, the necessary cooling for the SQUID could be easily combined with the existing cryostat.

Another way to solve the problem of measuring the tunnel-gap resistance at high bandwidth was recently proposed by Kamiktarkak *et al.* [80]. By making the tunnel junction resistance part of a resonant RLC circuit (resistor-inductor-capacitor) that terminates a coaxial cable, they monitor the change in radio frequency (RF) reflectivity as the tunnel junction resistance changes. In this way, they demonstrated very large bandwidths for low tunnel junction resistances (between 100 k $\Omega$  and 10 M $\Omega$ ). However, the application of this method becomes less favorable for larger tunnel junction resistances. For a typical tunnel junction of 1 G $\Omega$ , which is necessary to reduce tip influences on the surface atoms, it is again hardly possible to reach a bandwidth of 1 MHz. Moreover, when applying tunnel settings such that the junction resistance is lower than 10 M $\Omega$ , there is no need to use a large feedback resistor in the I/V-converter like the common standard of 1 G $\Omega$ . After all, it is not necessary to build an I/V converter with a noise figure much better than the thermal noise of the tunnel junction itself. One might just as well build an I/V converter with a feedback resistor that itself is 10 M $\Omega$ , which reduces many of the complications involved in building a large bandwidth I/V converter.

### 4.2 Non-linear coupling of piezo movements

In Section 3.2 we demonstrated the undesired generation of non-linear movements of the piezo scanning element. This effect has a quite serious consequence for (fast) SPM measurements: even when the scan operation is performed with a perfect sine-shaped signal, the driving signal will mix with all other frequency components at which the actuator moves. As this motion also includes the height correction ( $Z$ -motion) that is controlled by the feedback, it generates an unwanted motion at both higher and lower frequencies than the scan frequency. This will lead to a serious problem, if one of those frequencies does match with one of the natural resonance frequencies of the system. As additional energy is pumped into this particular mode, it also limits the possible maximum gain settings of the feedback before the circuit becomes unstable thereby reducing both resolution and speed. The obvious and easiest solution to this problem is given by the selection of piezo-actuators with a first natural resonance frequency, which is as high as possible, making conical scanners (see above) or stack scanners preferential to the standard cylindrical ones. More advanced solutions might be smart signal processing of the driving signals.

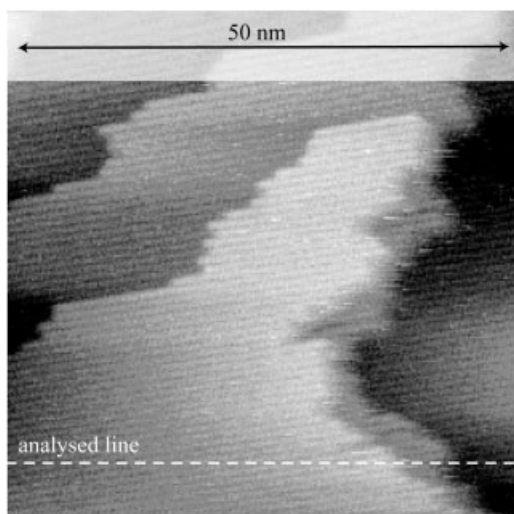


Fig. 8. STM image that was used for the feedback analysis mentioned in the text. The image was recorded at  $I = 100$  pA,  $V = -1.5$  V, and line-rate of 36 Hz. This image was scanned left-to-right ('trace'). The dashed line marks the location on which the analysis was performed.

### 4.3 Vertical speed (acceleration) limit

One of the central issues in the context of video-rate imaging is the speed at which the position of the scanning probe can be adapted to changes in the probe-surface distance. Obviously, this speed depends on the loop gain settings of the feedback circuit. In the following experiment we demonstrate one of the major limiting aspects of conventional feedback systems: the acceleration limit.

We prepared an atomically flat, but stepped Au (110) single crystal surface in an ultra high vacuum STM. The STM image of Fig. 8 shows three atomic layers consisting of atom rows (almost horizontal lines) that are typical for the so-called 'missing-row reconstruction' of this particular surface. As is the case in most experiments, the surface normal of the sample is slightly misaligned with respect to the  $Z$ -actuation direction of the piezo element resulting in a sloped background (for display reasons, this background is subtracted in Fig. 8). The field of view of this image is  $50 \times 50$  nm<sup>2</sup>. We analyzed a line trace as indicated by the dashed line in the figure: the total height variation is 4.4 nm over the entire scan line of 50 nm including two atomic steps. Without changing the feedback parameters, the exact same location was scanned at various tip speeds corresponding to line-rates ranging from 36 Hz to 217 Hz or 6.8 sec/image to 0.85 sec/image respectively.

For every line-rate, we analyzed the trace and retrace height line at the fixed position indicated in the

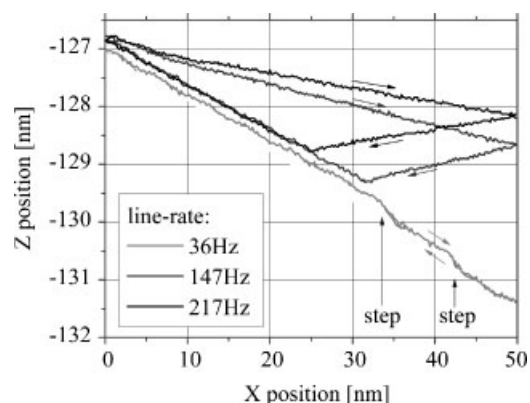


Fig. 9. Three examples of line scans taken with different tip speeds at the position of the dashed line in Fig. 8. The scan direction is illustrated by the arrows. We also indicated the two steps in the surface in the scan at 36 Hz.

image. Three examples of those line-scans recorded at three different line-rates are shown in Fig. 9. The arrows in the figure represent the scan-direction; the corresponding line rates are indicated.

The tip perfectly follows the surface at the lowest line-rate, both for the 'uphill' trace and the 'downhill' trace. At this speed, the positions of two steps in the surface are imaged perfectly for both directions indicating good control by the feedback. On increasing the line speed, we find that at some moment the tip can not follow the surface anymore on its way downhill. For a major part of the scan, the tip loses the tunneling regime, thereby eventually reaching a tip-sample separation of more than 3 nm! The tip, however, is still steered back to the surface by the feedback circuit with a constant velocity  $v_{\text{down}}$ . At a certain moment, after the scan-direction is reversed, the tip reenters the tunneling regime, and properly follows the surface uphill. Considering this observation, we would like to point out two striking features. First, the feedback circuit is not capable of following the surface downhill, while it does follow the surface perfectly uphill. At first sight this might seem contradictory. Second, when losing the tunneling regime the tip is steered towards the surface with a constant speed.

We can explain this behavior in terms of a strongly non-linear dependence of the input signal of the feedback with respect to the tip-sample distance. Although the exponential behavior of the tunneling current with respect to tip-sample separation is almost perfectly liberalized by the logarithmic amplifier in our feedback-input stage, the input signal drops to zero and stays zero as long as the system is out of the tunneling regime independent of the actual tip-sample distance.

In addition, due to the noise generated in the preamplifier, which is later rectified by an absolute value converter, the input of the feedback detects a finite artificial tunneling current, although the tip is out of the tunneling regime.  $V_{\text{down}}$  is determined by the difference between the tunneling-current setpoint and the artificial created tunneling current multiplied by the feedback gains. As long as the STM is out of the tunneling regime, this difference will be constant. The proportional action of the feedback on this constant leads to a constant output voltage for the  $Z$  actuation, while the integrating gain leads to an output signal that grows linearly in time. Therefore, the position of the tip will move linearly back towards the surface, *i.e.*  $V_{\text{down}}$  is constant. Please note that in our case the maximum speed is  $v_{\text{down,max}} \approx 575$  nm/sec, which is not at all an impressively high velocity. Theoretically, this speed could be increased by increasing the I-gain settings. However, as we already optimized the I-gain settings for stable scanning conditions, a further increase would result in an unstable, resonating feedback circuit and would eventually lead to tip-surface contact (tip crash) as soon as the tip gets into the tunneling regime again.

The fact that the tip is not crashed into the surface while scanning uphill can be understood by realizing that *approaching* the surface closer than the set-point value will lead to a linearly increasing error value (after the logarithmic amplifier) as long as the saturation value of the amplifiers has not been reached. This leads to an *increasing* speed  $v_{\text{up}}$  at which the tip is regulated away from the surface in contrast to the *constant* speed  $v_{\text{down}}$ , with which the tip is steered towards the surface. Considering extreme situations, in which the tunneling current exceeds the corresponding saturation voltage of the amplifiers, the tip is retracted eventually with a *constant* velocity  $v_{\text{up}}$ . This speed depends on the difference between the saturation voltage and the set-point value. Finally, one should realize that the maximum velocities for the upwards and downwards movements will always differ, as long as the setpoint value (asked tunneling current) deviates from the middle of the dynamic regime of the amplifiers taking into account also the noise generated in the preamplifier.

The above described problem of a non-linear error signal is not only limited to STM experiments; it is also encountered in dynamic mode AFM measurements, where the amplitude of the cantilever oscillations is used as a feedback input signal. As long as the distance to the surface is larger than the range of the interactions, the cantilever will oscillate at its 'free-amplitude' resulting in a constant input for the feedback. It is possible to minimize this problem by implementing a non-linear gain in the feedback circuit [58]. The feedback gains

should increase strongly as soon as the input signal for the feedback saturates to a constant value.

To summarize this section, we demonstrated that the maximum speed of an SPM can be limited by the fact that the signal, which is used for the feedback, can be a strongly non-linear function of the probe-surface separation. In an STM-experiment for example, this will especially limit the imaging of rough surfaces at low current settings.

## V. PROSPECTIVE

### 5.1 Micro-Electro-Mechanical Systems (MEMS) scanners

The speed of an SPM system is limited by the mechanical resonances of the scanner. Especially, the resonance in  $Z$  (height) is important, as the motion in the  $Z$ -direction is usually the fastest and requires the highest frequency components. Typical SPM scanners have a  $Z$ -resonance frequency around 50 kHz (see above), which limits the usable speed of the SPM even if the control electronics are faster.

To obtain faster scan speeds in the  $Z$ -direction, we have set up a research program to develop MEMS (micro-electromechanical systems) scanners. MEMS are small machines that have a mechanical functionality and are made with techniques comparable to those that are used to manufacture semiconductor chips. Until now, MEMS-SPM research has been mainly focused on applications directed towards an array or matrix of scanners with AFM functionality. Such arrays could be used for data storage applications: the IBM millipede project being the most widely known example [81–85]. Single MEMS scanners have also been fabricated in the past but their relatively low resonance frequencies prevented users from applying these scanners a lot in practice. An example is shown in Fig. 10 [86–90].

However, small MEMS stages with limited range (a few hundred nanometers) can have fundamental resonances well into the MHz range, potentially enabling extremely rapid scanning. An additional advantage of a MEMS scanner is the extremely small moving mass. Compared to common piezo scanners, significantly less vibrational energy is coupled into the system, which can excite lower mechanical resonances elsewhere in the microscope. Also, superior to the (voltage driven) piezo scanner, the MEMS scanner operates without hysteresis. At the University of Leiden, we are currently developing MEMS devices to provide the  $Z$ -axis motion of an SPM instead of using a conventional scanner (see Fig. 11a). Preliminary results with one of our prototypes show high fundamental resonances in the order of a few

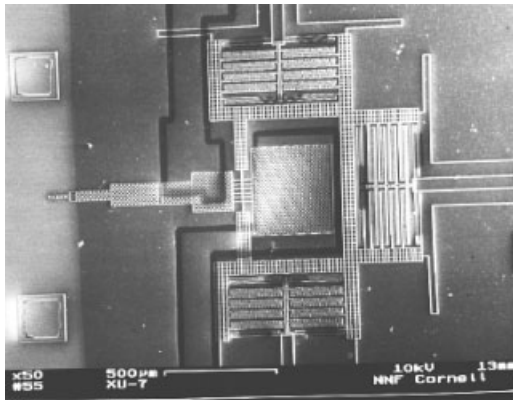


Fig. 10. MEMS XYZ scanner of Cornell University; reproduced with permission [86].

hundred kHz to the low MHz range and a quality factor  $Q$  in the order of 10 (see Fig. 11b). We have implemented a high-speed AFM with a MEMS Z-stage, of which the results will be published later [91].

We expect that MEMS scanners will enable a wide variety of high-speed SPM experiments that are impossible today. As the MEMS scanner is very small (in our case, the stage size is typically between  $40 \times 40$  and  $100 \times 100 \mu\text{m}^2$ ), either a very small and light sample is required or a tip has to be manufactured on the MEMS itself. Both approaches may be feasible, although the tip-on-MEMS approach is currently considered to be the most user-friendly and generic.

## 5.2 Charge steering

One of the major current limitations in SPM is the non-linear response of the piezo scanner to the applied voltage coming from the driver amplifier (see above). This non-linear response causes hysteresis in the motion of the piezo scanner and excites higher harmonics of the driving signal in the motion, which can also excite mechanical resonances in the microscope long before the fundamental resonance frequency of the piezo has been reached. It, therefore, limits both the accuracy (not sensitivity) and the maximum usable scanning frequency of the microscope.

This non-linear behavior is caused by the fact that the piezo scanner responds to the exact charge on the electrodes, not the voltage across them. As the capacitance changes with the piezo motion, the charge on the scanner plates (which is the quantity normally controlled by the driver electronics) is not perfectly mirroring the voltage on the plates. It has been proposed to use driver electronics that control the charge rather than the voltage on a piezo for other applications, but it has not yet been implemented in a fully functional

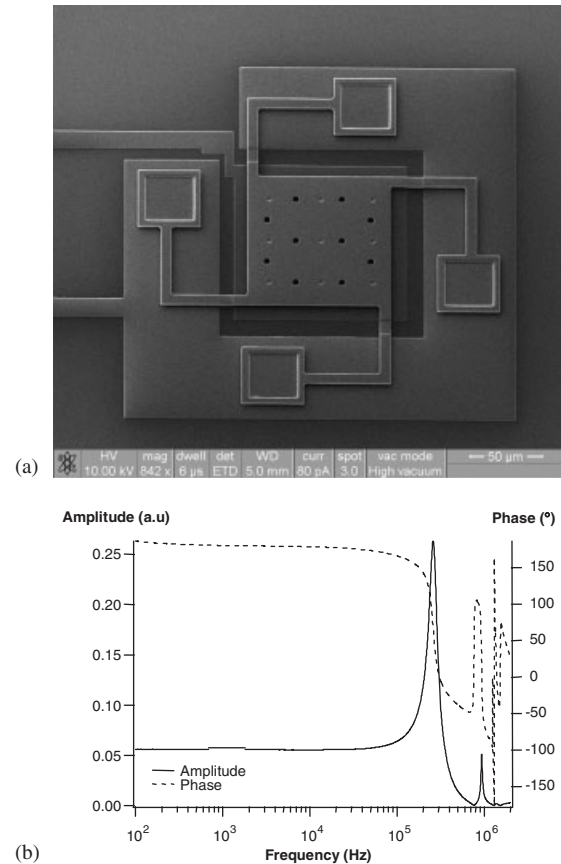


Fig. 11. (a) Scanning electron microscope (SEM) micrograph of the Leiden University MEMS scanner and (b) frequency response measured with an optical detection technique.

manner in scanning probe microscopes. From non-SPM measurements it is known that charge steering is very effective in reducing the piezo hysteresis [71, 92–94] (see Fig. 12).

Charge control (with a feedback loop sensitive to the charge on the piezo) can be achieved with an electronic circuit shown in Fig. 13 [93–95]. In Fig. 13(a), a voltage driver is shown, in which case the voltage on the piezo is proportional to the input voltage of the driver. In Fig. 13(b), the piezo is part of a feedback loop with a high-quality capacitor to ground. For an ideal operational (differential) amplifier (OpAmp), there will be no current flowing into the inverting input; hence the charge on the piezo will be exactly equal to the charge on the capacitor. The output will adjust its voltage until the inverting input (and hence the capacitor) carries the same voltage as the voltage applied to the non-inverting input. This corresponding charge  $Q$  on the capacitor, hence  $Q$  on the piezo, is given by  $Q = CV$ , where  $C$  is the capacitor value and  $V$  the applied voltage; the charge on the piezo is proportional to the input voltage as required for accurate charge control.

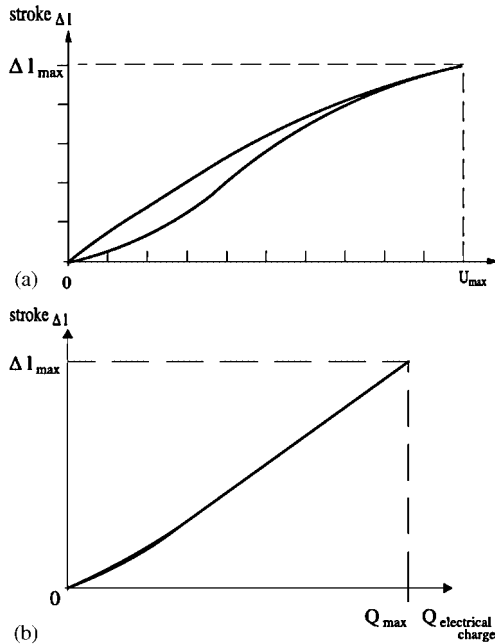


Fig. 12. Displacement of a piezo stack versus amplifier input signal by applying (a) a voltage controlled driver, and (b) a charge controlled driver. Charge control linearizes the mechanical response of a piezo. The graphs are reproduced with permission [92].

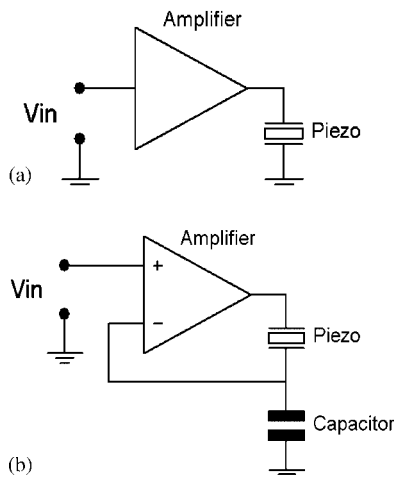


Fig. 13. (a) Voltage control and (b) charge control piezo driver principles.

Until now, charge steering has not been used in SPM technology because of practical challenges related to its operation. The charge driver is more complex than a voltage driver and charge steering is inherently unstable as time goes to infinity. Error sources in the circuit (*e.g.* the input bias current of the amplifier and leakage currents of both the capacitor and piezo) are integrated in a charge steering system until they dominate the overall behaviour. This means that in a practical system, a

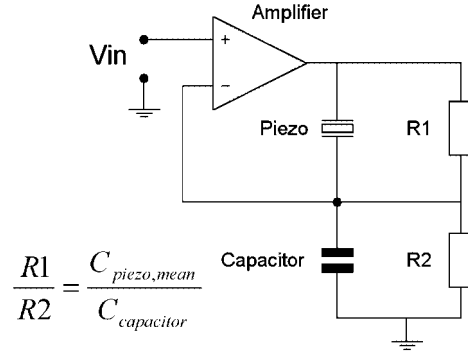


Fig. 14. For longer times, the charge control system becomes voltage-controlled in order to prevent instability of the circuit as time goes to infinity, see *e.g.* [96].

transition timescale has to be added such that the system behaves as a voltage driver for longer times (minutes to hours), see Fig. 14 [96]. As the required motions for imaging are relatively fast compared to this transition timescale, this solution should be considered, as it will improve hysteresis and non-linearity-induced resonances considerably.

Recently, Kageshima *et al.* [97] presented an approach where the piezo is voltage driven, but the charge on the piezo and the current flowing to the piezo are measured to provide information on the displacement and velocity of the piezo motion. These signals are then used as inputs for a local feedback loop controlling the piezo voltage driver. With this approach, they were not only able to reduce the linearity error to less than 1% but they also compensated for gain errors that are introduced due to the fundamental resonances of the piezo element by using the velocity signal.

### 5.3 Scanner engineering and model based controllers

Obviously, designing scanners with high resonance frequencies presents a good starting point. However, one still faces problems, *e.g.* non-linear couplings and vibrations that are coupled into the system by the scanning piezo element. These vibrations can excite lower mechanical resonances elsewhere in the microscope. Kodera *et al.* [57] have shown that when special care is taken to counterbalance the actuator movements these unwanted resonances can be suppressed. They also have shown that higher gain settings of the feedback can be applied, when the piezo resonance is actively damped.

Another major step can be taken by characterizing the complete amplitude and phase behaviour of the scanning piezo element as a function of frequency and subsequently tailoring the voltage signals applied

to the piezo actuator taking into account its specific behaviour. In this way, it is possible to apply a signal such that the piezo element exactly follows the desired movement. As an example, using a tailored driving voltage pulse, it is possible to counteract the overshoot of a piezo element that would occur when driving the piezo with a square wave. It is important to realize that such an application, called H-infinity, involves real-time processing of the desired signal: first the signal has to be Fourier transformed, then multiplied with the frequency dependent correction factors, after which a Fourier back-transformation results in the final signal, with which the piezo element is driven. Schitter *et al.* [46, 52, 53, 98] have impressively shown that system identification and subsequent implementation of an H-infinity controller can indeed improve the performance of a scanning probe microscope by a factor of five. Their implementation, using digital signal processing, requires quite extensive computing power. Applying modern FPGA technology, signal processing should be possible also for scanners that have resonance frequencies close to 1 MHz.

A similar, totally analog approach has been realized by Kodera [57]: they implemented an active damping scheme.

## VI. CONCLUSIONS

In conclusion, we have identified the most critical aspects that have to be addressed when speeding up SPM technology. We have reviewed both existing solutions and highlighted new innovative approaches.

Concerning the control electronics, new control concepts, like the hybrid mode, increase not only the resolution but also the possible maximum imaging speed of even existing microscopes. Future developments in electronic components will naturally provide new solutions for electronics that will have larger bandwidths combined with less noise. However, we believe that the desired requirements for preamplifiers (I/V-converters), which include the combination of low noise and large bandwidth, will still form a major bottleneck for STM. SQUID technology might offer a new solution. Concerning the possible data transfer, we believe that ongoing progress in network and communication developments will provide new solutions, although we are currently at the edge of what is possible. Long-term data storage, however, will remain a general problem.

Concerning the piezo scanning elements, we have shown that non-linearity is indeed a major issue regarding the performance of the microscopes. This non-linearity is capable of exciting resonances in the mechanical loop that are even lower than the lowest

resonance frequency of the piezo element itself. The first obvious solution is to use piezo elements with high natural frequencies, like the cone scanner which combine high resonance frequencies with sufficiently large scan ranges. However, at increased imaging speed, we have also shown that we face a speed limit in the vertical movement. This limit might be shifted to higher values when using light mass, high-frequency scanners, like the MEMS scanner.

Finally, we have reviewed smart driving signal solutions, like H-infinity, analog damping, and charge steering that all increase the performance of the piezo elements.

We believe that the combination of our hybrid mode and high-speed electronics, if equipped with an H-infinity solution to each of the drivers, will enable the next step in high-speed imaging with active feedback.

## REFERENCES

1. Young, R., J. Ward, and F. Scire, *Rev. Sci. Instrum.*, Vol. 43, p. 999 (1972).
2. Binnig, G., H. Rohrer, Ch. Gerber, and E. Weibel, *Phys. Rev. Lett.*, Vol. 49, p. 57 (1982).
3. Binnig, G. and H. Rohrer, *IBM J. Res. Dev.*, Vol. 30, p. 4 (1986).
4. Sagisaka, K., M. Kitahara, D. Fujita, G. Kido, and N. Koguchi, *Nanotechnology*, Vol. 15, p. S371 (2004).
5. Wiebe, J., A. Wachowiak, F. Meier, D. Haude, T. Foster, M. Morgenstern, and R. Wiesendanger, *Rev. Sci. Instrum.*, Vol. 75, p. 205411 (2004).
6. Rost, M. J., D. A. Quist, and J. W. M. Frenken, *Phys. Rev. Lett.*, Vol. 91, p. 026101 (2003).
7. Rasmussen, P. B., B. L. M. Hendriksen, H. Zeijlemaker, H. G. Ficke, and J. W. M. Frenken, *Rev. Sci. Instrum.*, Vol. 69, p. 3879 (1998).
8. Laegsgaard, E., L. Osterlund, P. Thostrup, P. B. Rasmussen, I. Stensgaard, and F. Besenbacher, *Rev. Sci. Instrum.*, Vol. 72, p. 3537 (2001).
9. Sonnenfeld, R. and P. K. Hansma, *Science*, Vol. 232, p. 211 (1986).
10. Pivetta, M., M. Ternes, F. Patthey, and W.-D. Schneider, *Phys. Rev. Lett.*, Vol. 99, p. 126104 (2007).
11. Bode, M., M. Heide, K. von Bergmann, P. Ferriani, S. Heinze, G. Bihlmayer, A. Kubetzka, O. Pietzsch, S. Blügel, and R. Wiesendanger, *Nature*, Vol. 447, No. 193, p. 190 (2007).
12. Manoharan, H. C., C. P. Lutz, D. M. Eigler, *Nature*, Vol. 403, p. 512 (2000).
13. Marczinowski, F., J. Wiebe, J.-M. Tang, M. E. Flatté, F. Meier, M. Morgenstern, and

- R. Wiesendanger, *Phys. Rev. Lett.*, Vol. 99, p. 157202 (2007).
14. Hirjibehedin, C. F., C. Y. Lin, A. F. Otte, M. Ternes, C. P. Lutz, B. A. Jones, A. J. Heinrich, *Science*, Vol. 317, p. 1199 (2007).
  15. Viani, M. B., L. I. Pietrasanta, J. B. Thompson *et al.*, *Nature Struct. Biol.*, Vol. 7, p. 644 (2000).
  16. Ando, T., N. Kodera, E. Takai, D. Maruyama, K. Saito, and A. Toda, *Proc. Natl. Acad. Sci. U.S.A.*, Vol. 98, p. 12468 (2001).
  17. www.realnano.nl; Dutch research initiative on “Nanoimaging under Industrial Conditions”; last visited March 11, 2009.
  18. Pantazi, A., M. A. Lantz, G. Cherubini, H. Pozidis, and E. Eleftheriou, *Nanotechnology*, Vol. 15, p. S612 (2004).
  19. www.mapperlithography.com/; MAPPER Lithography B.V., Delft, the Netherlands; last visited March 11, 2009.
  20. Wilson, J. and C. de Groot, *J. Phys. Chem.*, Vol. 99, p. 7860 (1995).
  21. Dimension 5000, Digital Instruments, Veeco.
  22. Rost, M. J., *Phys. Rev. Lett.*, Vol. 99, p. 266101 (2007).
  23. Hoogeman, M. S., *et al.*, *Rev. Sci. Instrum.*, Vol. 69, p. 2072 (1998).
  24. Frenken, J. W. M. and B. L. M. Hendriksen, *MRS Bull.*, Vol. 32, p. 1015 (2007).
  25. Hendriksen, B. L. M. and J. W. M. Frenken, *Phys. Rev. Lett.*, Vol. 89, p. 046101 (2002).
  26. Hendriksen, B. L. M., S. C. Bobaru, and J. W. M. Frenken, *Catal. Today*, Vol. 105, p. 234 (2005).
  27. Ando, T., T. Uchihashi, N. Kodera, A. Miyagi, R. Nakakita, H. Yamashita, and M. Sakashita, *Jpn. J. Appl. Phys.*, Vol. 45, Part 1, p. 1897 (2006).
  28. Ando, T., T. Uchihashi, N. Kodera, D. Yamamoto, A. Miyagi, M. Taniguchi, and H. Yamashita, *Eur. J. Physiol.*, Vol. 456, p. 211 (2008).
  29. Yamashita, H., N. Kodera, A. Miyagi, T. Uchihashi, D. Yamamoto, and T. Ando, *Rev. Sci. Instrum.*, Vol. 78, p. 083702 (2007).
  30. Kuipers, L., M. S. Hoogeman, J. W. M. Frenken, and H. van Beijeren, *Phys. Rev. B*, Vol. 52, p. 11387 (1995).
  31. Rost, M. J. and J. W. M. Frenken, *Phys. Rev. Lett.*, Vol. 87, p. 039603 (2001).
  32. Kuipers, L., R. W. M. Loos, H. Neerings, J. ter Horst, G. J. Ruwiel, A. P. de Jongh, and J. W. M. Frenken, *Rev. Sci. Instrum.*, Vol. 66, p. 4557 (1995).
  33. Ando, T., N. Kodera, D. Maruyama, E. Takai, K. Saito, and A. Toda, *Jpn. J. Appl. Phys.*, Vol. 41, Part 1, p. 4851 (2002).
  34. Kindt, J. H., G. E. Fantner, J. A. Cutroni, and P. K. Hansma, *Ultramicroscopy*, Vol. 100, p. 259 (2004).
  35. Curtis, R., T. Mitsui, and E. Ganz, *Rev. Sci. Instrum.*, Vol. 68, p. 2790 (1997).
  36. Humphris, A. D. L., J. K. Hobbs, and M. J. Miles, *Appl. Phys. Lett.*, Vol. 83, p. 6 (2003).
  37. Gesquiere, A., M. M. Abdel-Mottaleb, S. de Feyter, F. C. de Schryver, M. Sieffert, K. Mullen, A. Calderone, R. Lazzaroni, J. L. Bredas, *Chem. A – Eur. J.*, Vol. 6, p. 3739 (2000).
  38. Schitter, G. and M. J. Rost, *Materials Today* (in press).
  39. Schitter, G. and A. Stemmer, *IEEE Trans. Control Syst. Technol.*, Vol. 12, p. 449 (2004).
  40. Rost, M. J., *et al.*, *Rev. Sci. Instrum.*, Vol. 76, p. 053710 (2005).
  41. Fantner, G. E., P. Hegarty, J. H. Kindt, G. Schitter, G. A. G. Cidade, and P. K. Hansma, *Rev. Sci. Instrum.*, Vol. 76, p. 026118 (2005).
  42. Zou, Q. Z. and S. Devasia, *IEEE Trans. Control Syst. Technol.*, Vol. 12, p. 375 (2004).
  43. Yan, Y., Y. Wu, Q. Z. Zou, and C. M. Su, *Rev. Sci. Instrum.*, Vol. 79, p. 073704 (2008).
  44. Salapaka, S., A. Sebastian, J. P. Cleveland, and M. V. Salapaka, *Rev. Sci. Instrum.*, Vol. 73, p. 3232 (2002).
  45. Leang, K. K. and S. Devasia, *IEEE Trans. Control Syst. Technol.*, Vol. 15, p. 927 (2007).
  46. Schitter, G., P. J. Thurner, and P. K. Hansma, *Mechatronics*, Vol. 18, p. 282 (2008).
  47. Schitter, G., F. Allgöwer, and A. Stemmer, *Nanotechnology*, Vol. 15, p. 108 (2004).
  48. Michely, T., M. Kaiser, and M. J. Rost, *Rev. Sci. Instrum.*, Vol. 71, p. 4461 (2000).
  49. Hansma, P. K., G. Schitter, G. E. Fantner, and C. Prater, *Science*, Vol. 314, p. 601 (2006).
  50. Schitter, G., K. J. Åström, B. E. DeMartini, P. J. Thurner, K. L. Turner, and P. K. Hansma, *IEEE Trans. Control Syst. Technol.*, Vol. 15, p. 906 (2007).
  51. Picco, L. M., L. Bozec, A. Ulcinas, D. J. Engledew, M. Antognozzi, M. A. Horton, and M. J. Miles, *Nanotechnology*, Vol. 18, p. 044030 (2007).
  52. Schitter, G., P. Menold, H. F. Knapp, F. Allgöwer, and A. Stemmer, *Rev. Sci. Instrum.*, Vol. 72, p. 3320 (2001).
  53. Schitter, G., A. Stemmer, and F. Allgöwer, *Asian J. Control*, Vol. 6, p. 156 (2004).
  54. Libioulle, L., A. Radenovic, E. Bystrenova, and G. Dietler, *Rev. Sci. Instrum.*, Vol. 74, p. 1016 (2003).
  55. Hosaka, S., T. Hasegawa, S. Hosoki, and K. Takata, *Rev. Sci. Instrum.*, Vol. 61, p. 1342 (1990).

56. [www.leidenprobemicroscopy.com](http://www.leidenprobemicroscopy.com); Leiden Probe Microscopy B.V., Leiden, The Netherlands; last visited March 11, 2009.
57. Kodera, N., H. Yamashita, and T. Ando, *Rev. Sci. Instrum.*, Vol. 76, p. 053708 (2005).
58. Kodera, N., M. Sakashita, and T. Ando, *Rev. Sci. Instrum.*, Vol. 77, p. 083704 (2006).
59. Uchihashi, T., N. Kodera, H. Itoh, H. Yamashita, and T. Ando, *Jpn. J. Appl. Phys.*, Vol. 45, Part 1, p. 1904 (2006).
60. Pilkey, W. D., *Stress, Strain, and Structural Matrices*, Wiley, New York (1994).
61. Kokavecz, J., O. Marti, P. Heszler, and A. Mechler, *Phys. Rev. B*, Vol. 73, p. 155403 (2006).
62. Walters, D. A., J. P. Cleveland, N. H. Thomson, P. K. Hansma, M. A. Wendman, G. Gurley, and V. Elings, *Rev. Sci. Instrum.*, Vol. 67, p. 3583 (1996).
63. Paloczi, G. T., B. L. Smith, P. K. Hansma, D. A. Walters, and M. A. Wendman, *Appl. Phys. Lett.*, Vol. 73, p. 1658 (1998).
64. Viani, M. B., T. E. Schaffer, A. Chand, M. Rief, H. E. Gaub, and P. K. Hansma, *J. Appl. Phys.*, Vol. 86, p. 2258 (1999).
65. Chand, A., M. B. Viani, T. E. Schaffer, and P. K. Hansma, *J. Microelectromech. Syst.*, Vol. 9, p. 112 (2000).
66. Kitazawa, M., K. Shiotani, and A. Toda, *Jpn. J. Appl. Phys.*, Vol. 42, Part 1, p. 4844 (2003).
67. Sader, J. E., *J. Appl. Phys.*, Vol. 84, p. 64 (1998).
68. Katan, A. J. and T. H. Oosterkamp, *J. Phys. Chem. C*, Vol. 112, p. 9769 (2008).
69. Yang, J. L., M. Despont, U. Drechsler, B. W. Hoogenboom, P. L. T. M. Frederix, S. Martin, A. Engel, P. Vettiger, and H. J. Hug, *Appl. Phys. Lett.*, Vol. 86, p. 134101 (2005).
70. [www.eblproducts.com](http://www.eblproducts.com), EBL Products INC., East Hartford, U.S.A.; last visited March 11, 2009.
71. Moheimani, S. O. R., *Rev. Sci. Instrum.*, Vol. 79, p. 071101 (2008).
72. van Loo, W. A., to be published.
73. Fantner, G. E., G. Schitter, J. H. Kindt, T. Ivanov, K. Ivanova, R. Patel, N. Holten-Andersen, J. Adams, P. J. Thurner, I. W. Rangelow, and P. K. Hansma, *Ultramicroscopy*, Vol. 106, p. 881 (2006).
74. Kodera, N., Y. Naito, T. Ito, and T. Ando, *Biophys. J.*, Vol. 84, p. 467A (2003).
75. Aphale, S., B. Bhikkaji, and S. O. R. Moheimani, *IEEE Trans. Nanotechnol.*, Vol. 7, p. 79 (2008).
76. Fukuma, T., Y. Okazaki, N. Kodera, T. Uchihashi, and T. Ando, *Appl. Phys. Lett.*, Vol. 92, p. 243119 (2008).
77. Humphris, A. D. L., M. J. Miles, and J. K. Hobbs, *Appl. Phys. Lett.*, Vol. 86, p. 034106 (2005).
78. Picco, L. M., P. G. Dunton, A. Ulcinas, et al., *Nanotechnology*, Vol. 19, p. 384018 (2008).
79. Kalabukhov, A., L. Kuzmin et al., *Conference Proceedings of the Eur. Conf. Appl. Supercond. (EUCAS-2003)*, p. 3333 (2003).
80. Kemiktarak, U., T. Ndukum, K. C. Schwab, and K. Ekinici, *Nature*, Vol. 450, p. 85 (2007).
81. Mamin, H. J., L. S. Fan, S. Hoen, and D. Rugar, *Sens. Act. A*, Vol. 48, p. 215 (1995).
82. Miller, S. A., K. L. Turner, and N. C. MacDonald, *Rev. Sci. Instrum.*, Vol. 68, p. 4155 (1997).
83. Vettiger, P., M. Despont, U. Drechsler, U. Dürig, W. Häberle, M. I. Lutwyche, H. E. Rothuizen, R. Stutz, R. Widmer, and G. K. Binnig, *IBM J. Res. Develop.*, Vol. 44, No. 3, p. 323 (2000).
84. Shin, H., S. Hong, J. Moon, and J. U. Jeon, *Ultramicroscopy*, Vol. 91, p. 103 (2002).
85. Ahn, Y., T. Ono, and M. Esashi, *J. Micromech. Microeng.*, Vol. 15, p. 1224 (2005).
86. MacDonald, N. C., *Microelectron. Eng.*, Vol. 32, p. 49 (1996).
87. Akamine, S., T. R. Albrecht, M. J. Zdeblick, and C. F. Quate, *IEEE Electron Device Lett.*, Vol. 10, p. 490 (1989).
88. Indermühle, P.-F., V. P. Jaecklin, J. Brugger, C. Linder, N. F. de Rooij, and M. Binggeli, *Sens. Act. A*, Vol. 46, p. 562 (1995).
89. Bay, J., S. Bouwstra, E. Lægsgaard, and O. Hansen, *J. Micromech. Microeng.*, Vol. 5, p. 161 (1995).
90. Sulchek, T., S. C. Minne, J. D. Adams, D. A. Fletcher, A. Atalar, C. F. Quate, and D. M. Anderton, *Appl. Phys. Lett.*, Vol. 75, p. 1637 (1999).
91. Disseldorp, E. C. M., et al., to be published.
92. "Piezomechanics: An Introduction," downloadable at [www.piezomechanik.com](http://www.piezomechanik.com), Piezomechanik GmbH, Munich - Germany.
93. Fleming, A. J. and S. O. R. Moheimani, *Rev. Sci. Instrum.*, Vol. 76, p. 073707 (2005).
94. Bhikkaji, B., M. Ratnam, A. J. Fleming, and S. O. R. Moheimani, *IEEE Trans. Control Syst. Technol.*, Vol. 15, p. 853 (2007).
95. Main, J. A., E. Garcia, and D. V. Newton, *J. Guid. Control Dyn.*, Vol. 18, No. 5, p. 1068 (1995).
96. Holterman, J., Vibration control of high-precision machines with active structural elements, *Ph.D. Thesis*, University of Twente, The Netherlands, p. 73 (2002).
97. Kageshima, M., S. Togo, Y. J. Li, Y. Naitoh, and Y. Sugawara, *Rev. Sci. Instrum.*, Vol. 77, p. 103701 (2006).
98. Stemmer, A., G. Schitter, J. M. Rieber, and F. Allgöwer, *Eur. J. Control*, Vol. 11, p. 384 (2005).



**Marcel J. Rost** received his MSc in physics from the University of Bonn, Germany, in 1996. The work of his master thesis, which included the design of an STM, was performed at the IGV, Forschungszentrum Jülich, Germany. He started his PhD at the AMOLF-FOM-institute, Amsterdam, and graduated in 2001. Being a co-founder of LPM, he also was the first CEO. Now he is an assistant professor at the Kamerlingh Onnes Laboratory, University of Leiden, The Netherlands. His research focuses on surface science and nanotechnology, especially on the evolution of polycrystalline thin films during growth/deposition and during a post-deposition treatment or application.



**Gertjan van Baarle** received his M.Sc (2000) and Ph.D. in physics (2005) from Leiden University. In 2005 he joined the Interface Physics group at Leiden University, concentrating on the development of high-speed SPM technology. Currently he is director of Leiden Probe Microscopy BV where he is working on the development and commercialisation of high-end tools for nano-science and technology, including fast SPM.



**Allard Katan** obtained an M.Sc. at Delft University of Technology and a Ph.D. at Leiden University. Currently he is a post-doc at the Interface Physics group at Leiden University working on the development and application of high-sensitivity and high-speed Atomic Force Microscopy.



**W. Merlijn van Spengen** received the M.S. degree in electronic engineering from Eindhoven University of Technology, The Netherlands, in 1999. In 2004 he obtained the Ph.D. degree from the Catholic University of Leuven, Belgium, while staying at the independent microelectronics research institute

IMEC. For his Ph.D. research he studied MEMS reliability. He is currently associated with Leiden University, The Netherlands, where he is working on MEMS tribology research and recently obtained the “discoverer of the year” award of the faculty of science. He is also director of the company Falco Systems.



**Peter Schakel** received his B.Sc. degree in Electrical Engineering from the H.T.S. Haarlem, the Netherlands. He has been working on electronics for several research projects in the field of chemistry and physics. Since 2007 he has been an engineer at the Nuclear-physics Accelerator Institute (KVI - Kernfysisch Versneller Instituut) in Groningen.



**W. A. van Loo** received his M.S. degree in physics from Leiden University, The Netherlands in 2004. He continued working as a researcher for Leiden University until 2008. He is currently working at Rijkswaterstaat as a traffic expert improving the traffic flow at crossjunctions.



**Tjerk Oosterkamp** received his PhD in physics from the Technical University of Delft, the Netherlands. Now he is associate professor at the Leiden Institute of Physics of Leiden University, the Netherlands. His research focuses on high speed and high sensitivity AFM in liquid environments, and their application to physical and biomedical problems.



**Joost Frenken** carried out his Ph.D. research at the FOM-Institute for Atomic and Molecular Physics in Amsterdam and obtained his Ph.D. degree in 1986 from the University of Utrecht. Prior to his appointment in 1994 as a professor at Leiden University, he worked as an

Alexander-von-Humboldt Fellow in Gttingen and as a Huygens Fellow in Amsterdam. Frenken serves on a variety of national and international committees and boards and is the scientific director of the Dutch NIMIC-consortium: *Nano-Imaging under Industrial Conditions*. Central to the research of Joost Frenken are the

dynamic aspects of surfaces and interfaces. Topics of interest include surface diffusion, crystal growth, surface phase transitions, model catalysis, nanotribology, and biomembranes. For tailor-made measurements in each of these areas, Frenken's research group has developed a variety of special-purpose scanning probe microscopes.